Regular Article

PHYSICAL CHEMISTRY RESEARCH
Published by the
Iranian Chemical Society
www.physchemres.org
info@physchemres.org

Phys. Chem. Res., Vol. 12, No. 2, 419-428, June 2024
DOI: 10.22036/pcr.2023.397652.2342

Synthesis of Reduced Graphene Oxide/Hexagonal Boron Nitride Nanocomposite as Efficient Hydrogen-Storage Medium for Fuel Cell Applications

R. Naresh Muthu*

Department of Physics, J P College of Arts and Science, Tenkasi-627852, Tamil Nadu
(Affiliated to Manonmaniam Sundaranar University, Tirunelveli, Tamil Nadu)
(Received 18 May 2023, Accepted 13 September 2023)

In the present research, reduced graphene oxide (RGO) and hexagonal boron nitride (h-BN) nanoparticles-decorated RGO sheets for a solid-state hydrogen storage medium were synthesized and characterized. The nanocomposite of RGO/h-BN was prepared using the ultrasonic-assisted liquid-phase exfoliation approach and the modified Hummer's method was used for the synthesis of graphene oxide (GO). Using micro-Raman spectroscopy, XRD, SEM, CHNS elemental analysis, and TGA, the produced RGO and RGO/h-BN nanocomposites were analyzed. XRD and micro-Raman validated the RGO and the RGO decorated with h-BN nanoparticles. SEM analysis authorized the h-BN nanoparticles that were decorated on the surface of the RGO sheet. Using a hydrogenation system akin to Sievert's, the hydrogen adsorption behavior of the RGO and the RGO/h-BN nanocomposite was investigated. With a maximal hydrogen absorption of 2.1 wt% at 100 °C, RGO/h-BN nanocomposite performed better than the bare RGO. In the temperature ranges of 109° to 140° and 115° to 149°, the RGO and RGO/h-BN nanocomposites released 100% of the stored hydrogen. The corresponding binding energy of RGO and RGO/h-BN nanocomposites were 0.31 and 0.32 eV, which is adequate for fuel cell applications. The RGO/h-BN nanocomposite is therefore anticipated to have a promising future in hydrogen storage situations of fuel cell applications.

Keywords: h-BN (hexagonal boron nitride), RGO (reduced graphene oxide), RGO/h-BN nanocomposite, Hydrogen storage

INTRODUCTION

The prolonged usage of nonrenewable sources like fossil fuel emits greenhouse gases into the environment and is considered the root cause of the world's global warming problem. To meet our everyday needs, the scientific community is compelled to look for new and clean energy sources [1-3]. Water is the only byproduct of hydrogen, believed to be the purest and most renewable energy. However, the stored hydrogen must fulfill US-DOE's targets in 2025 [4]. Intense investigations have been focused on realizing a recovering hydrogen-storage system for fuel cell technology [5].

Compressed, liquid, and solid-state hydrogen are the three most common storage mechanisms currently employed [4]. In compressed and liquid hydrogen storage situations, dormancy and safety issues are significant factors in storing hydrogen for automobile usage. The best alternative is solid-state hydrogen storage since it has fewer safety concerns and a smaller design than high-pressure storage. Additionally, it is more affordable than the low-temperature process [6]. To date, massive attempts have been undertaken to store hydrogen in solid materials such as zeolites, carbon nanotubes, chemical hydrides, complex hydrides, metal hydrides, borohydrides, and organic-polymer networks. Despite the fact that many solid-state materials have substantial hydrogen storage capacities, releasing hydrogen can be expensive and requires a high desorption temperature, and some systems demonstrate irreversible hydrogen uptake [7-9]. Therefore, searching for safe and effective hydrogen storage materials is imperative to meet transportation requirements.

*Corresponding author. E-mail: rnaresh7708@gmail.com

Graphene, a single or few layers of graphite, is gaining popularity as a viable hydrogen storage media. A hexagonal honeycomb-shaped lattice of sp^2-bonded carbon atoms called graphene is a two dimensions (2D) material. [10]. This endows graphene's unique structure with excellent physicochemical properties such as lightweight, geometry, porous structures, high surface area, robustness, and chemical and thermal stability. These features make graphene a noteworthy candidate for hydrogen-storage systems [11-15]. Wang *et al.* [11] reported that graphene could store 0.9 wt% at 10 MPa (298 K). 1.2 wt% of hydrogen stored at 77 K and 10 bar in graphene nanosheets was observed by Srinivas *et al.* [12]. The thermal exfoliation of graphite oxide led to adsorption of 2.07 wt% at 50 bar (77 K) [13]. The hydrogen storage on Pd-N-HEG could be 4.4 wt% at 4 MPa and 25 °C [14]. RGO decorated with halloysite nanotube (RGO/A-HNT) nanocomposite showed 1.8 wt.% hydrogen-uptake capacity at 50 °C [15].

Recent research investigations demonstrate that employing BN (boron nitride) nanoparticles as a viable hydrogen-storage medium has sparked a lot of interest. H-BN (hexagonal boron nitride) is a material that resembles graphite in many ways, including its high specific surface area and mechanical strength, resistance to oxidation, and low density. Because of these critical tasks, h-BN is a viable choice for hydrogen storage [16-21]. Weng *et al.* [16] previously reported that the porous BN microbelts exhibited 2.3 wt% at 1 MPa and 77 K. The MWCNTs/h-BN nanocomposite shows 2.3 wt% hydrogen at 100 °C [17]. The hexagonal boron nitride (h-BN) and halloysite nanotubes (HNTs) nanocomposite had a 2.88 wt% hydrogen adsorption capacity at 50 °C [18]. The hydrogen-update capacity of straight-walled BNNTs, bamboo-type BNNTs, and BN nanostructures showed 3.0 wt%, 2.5 wt%, and 2.7 wt% at about 100 bar pressure. In contrast, [19] in BNNT collapsed walls, Tang *et al.* [20] discovered a hydrogen uptake of 4.2 wt% at 10 MPa. The BN whisker may absorb 5.6 wt% at ambient temperature (3 MPa), according to Li *et al.* report [21]. The challenge of developing a system for hydrogen-storage safely and effectively still lies ahead.

In response to these obstacles, the US-DOE Department of Energy aims to obtain 5.5 wt% gravimetric capacity by 2025 [22]. Only a few of the proposed hydrogen storage technologies can meet these criteria. Researchers are looking for an alternative method of producing hydrogen storage materials to solve this issue. To address the above-mentioned concerns, this research creates a safe, green, lightweight, and condensed hydrogen storage media based on RGO and h-BN nanoparticles decorated on RGO nanosheets (RGO/h-BN). Sonication-assisted liquid-phase exfoliation procedures were used to create the RGO/h-BN nanocomposites. Reduced graphene oxide (RGO) with a more excellent surface-to-volume ratio might store more hydrogen at all available hexagonal honeycomb structure adsorption sites. Because of the dipolar structure of B-N bonds in h-BN, hydrogen absorption is enhanced. Indeed, the lightweight RGO can absorb additional h-BN sequentially and additional hydrogen. Hydrogen-storage experiments at room temperature (100 °C) were conducted from the standpoint of practical applicability. This study demonstrates that RGO/h-BN nanocomposite is an excellent, cost-effective, and efficient choice for a solid-state hydrogen-storage system of fuel cell applications shortly.

EXPERIMENTAL

Chemicals

Sisco Research Laboratories and Loba provided h-BN (hexagonal boron nitride) nanoparticles and graphite powder. Merck offered H_2O_2 (hydrogen peroxide), DMF (N,N-dimethylformamide), H_2SO_4 (sulfuric acid), HCl (hydrochloric acid), $NaNO_3$ (sodium nitrate), N_2H_4 (hydrazine hydrate) and $KMnO_4$ (potassium permanganate). All of these compounds were of analytical grade and were not purified further. During these investigations, double-distilled water (H_2O) was utilized.

Synthesis of Reduced Graphene Oxide (RGO)

In an ice bath, graphite powder and $NaNO_3$ were added to 25 ml H_2SO_4 and stirred. The mixture above was then gradually added to $KMnO_4$ and stirred (1 hour) at 35 °C in a water bath. Apart from slowly adding 50 ml of water, the solution temperature rose to 98 °C. Finally, H_2O (100 ml) and H_2O_2 (10 ml) were further to the solutions described above. The solution was centrifuged, then washed by HCl (10%) and H_2O till the pH of the washing solution was nearly neutral. The resulting precipitate was vacuum-dried overnight at 40 °C before being crushed into a fine powder. The fine

powder was sonicated for one hour and thoroughly mixed with water. After some time, the solution above received the proper quantity of hydrazine hydrate. The precipitate was then collected and repetitively washed by ethanol and water. The powder that was created was then dried at 100 °C. RGO, or reduced graphene oxide, was the result.

Synthesis of RGO/h-BN Nanocomposite

The RGO/h-BN was prepared via a liquid-phase exfoliation process assisted by ultrasonic devices. In the conventional procedure, reduced graphite oxide (RGO) was fully dissolved in H_2O (1 mg ml^{-1}) and ultrasonically processed at RT. The solution was supplemented with h-BN nanoparticles (5 wt%), which were then stirred magnetically for 24 h. The mixture was then centrifuged to recover it and repeatedly rinsed in ethanol and water. The finished product was vacuum dried (60 °C) for an entire night before being annealed at 150 °C. The final product was referred to as RGO/h-BN nanocomposite.

Evaluation of Hydrogen Adsorption Activity

Hydrogenation setup method akin to Sieverts was used for the hydrogenation experiments. The procedure was as follows: the hydrogenation setup was examined for leaks prior to hydrogenation. In the hydrogenation chamber, the prepared RGO and RGO/h-BN nanocomposites were loaded. The chamber was then flushed with hydrogen gas three times after being vacuum-pumped out. Following the flushing procedure, the chamber was heated in a vacuum for 1 h at 100 °C. After that, hydrogen was applied to the prepared samples at a constant flow rate (0.5 l min^{-1}), and chamber pressure (1 kg cm^{-2}) was kept for 15 minutes. The amount of successfully adsorbed hydrogen was estimated once the samples had reached room temperature.

Materials Characterization

420 an X-ray diffractometer (XRD) with CuKα (X'Pert PAN analytical) at 2θ ranges from 10 to 80° at room temperature, the produced RGO and RGO/h-BN nanocomposite's crystalline structure was studied. Micro-Raman spectroscopy measurement was performed by LabRAM with 633 nm excitation at room temperature. The surface morphology was observed by JEOL-MODEL 6390 scanning electron microscope. Thermogravimetric analysis (TGA) was recorded by using SII EXSTAR 6000. The CHNS-elemental analysis was made by the Elementar Vario EL III model.

RESULTS AND DISCUSSION

Structural and Morphological Analysis

The XRD spectra of the RGO and the RGO/h-BN nanocomposites are exhibited in Fig. 1. Two diffraction peaks obtained in the XRD pattern of RGO at approximately 25.6° and 43.2°, which are attributed to the (002) and (100) planes (JCPDS card no. 75-2078). The diffraction peaks' broad nature shows the sheets' uneven arrangement along the stacking direction. It comprises a single or few layers of the less oxygen-containing functional group graphene sheet (RGO) [23]. It was also observed that the (002) plan exhibited a small shoulder peak, which might indicate the presence of graphite oxide (*i.e.*, thick graphene layer). Results for the RGO/h-BN (see Fig. 1b) showed that in addition to the RGO peaks, there were additional diffraction peaks visible at 26.3, 41.4, 43.5, 49.8, 54.8, and 75.8º, belonging to the diffraction crystal planes of (002), (100), (101), (102), (004) and (110), accordingly, which correspond to the h-BN (hexagonal phase boron nitrite) (JCPDS card no. 14-0033). No secondary diffraction peaks were observed, signifying that the single phase of h-BN nanoparticles exists in the prepared sample. The sharp diffraction validated that the well-crystalline h-BN nanoparticles were decorated on the surface of RGO. The absence of minor extra peaks proves the produced nanocomposites' purity and the production of RGO/h-BN.

The nanocomposite's crystalline size (D) is computed by the following Scherrer's Eq. (1) [17]:

$$D = 0.9\lambda/\beta \cos\theta \quad (1)$$

In above formulation, λ is the X-ray wavelength, β is the FWHM (full width at half maximum), and θ is the diffraction angle. The estimated crystalline size for RGO and RGO/h-BN nanocomposites is 7.27 and 7.48 nm, respectively.

The most effective method for identifying structural alterations in materials based on graphene is Raman spectroscopy. The micro-Raman spectra of produced RGO and RGO/h-BN are shown in Fig. 2. RGO (Fig. 2a) and

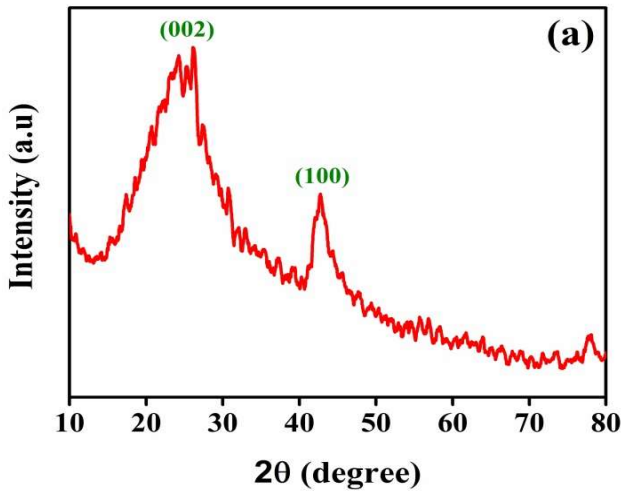

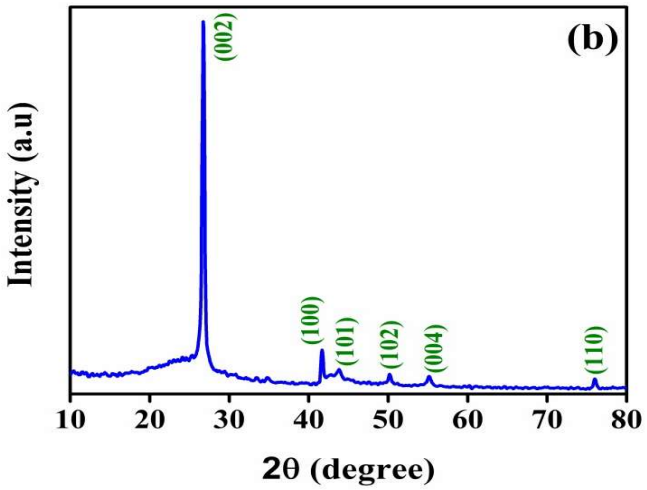

Fig. 1. XRD patterns of (a) RGO (b) RGO/h-BN hybrid nanocomposite.

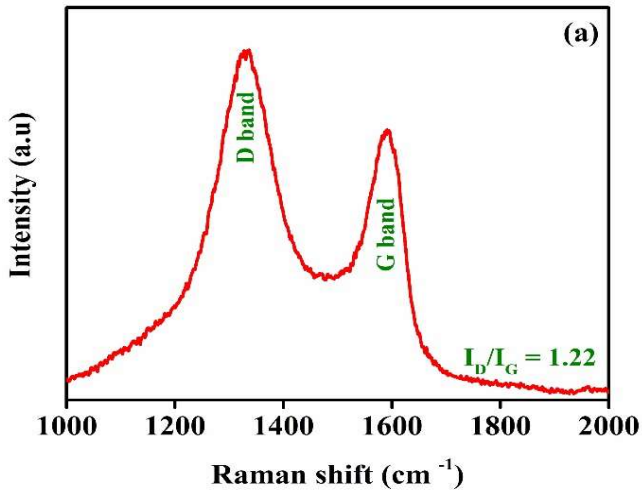

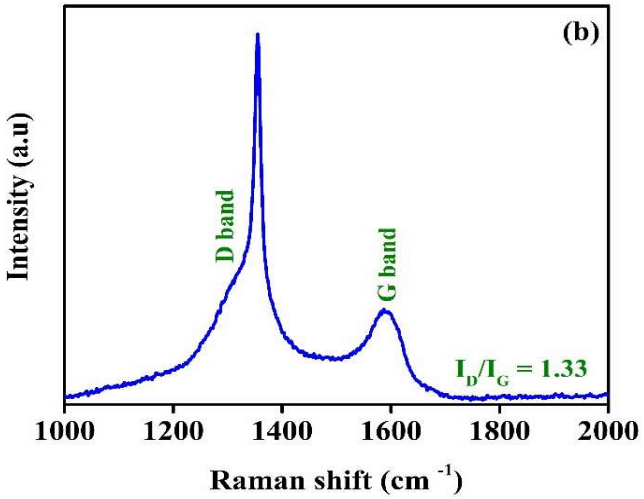

Fig. 2. Micro-Raman spectra of (a) RGO (b) RGO/h-BN nanocomposite.

RGO/h-BN nanocomposite (Fig. 2b) exhibited the two key characteristics, the D and G bands. The 1570 cm^{-1} (G band) is caused by the first-order scatter of the E_{2g} phonon, and the 1350 cm^{-1} (D band) is k-point phonons with A_{1g} symmetry [24,25]. The in-plane vibration of the B and N atoms (E_{2g} mode), which is also shown in Fig. 2b [26], corresponds to a new sharp, unique Raman feature at 1355 cm^{-1} along with the D and G band. This finding suggests that h-BN nanoparticles were decorated on the surface of two-dimensional RGO sheets, which is in agreement with the previously published studies.

The structural quality and degree of disorder of synthesized RGO and RGO/h-BN nanocomposites were determined by the peak intensity ratios of the D band to the G band (I_D/I_G). The estimated I_D/I_G of RGO and RGO/h-BN nanocomposites were 1.22 and 1.33, respectively. From Fig. 2, the I_D/I_G of RGO/h-BN nanocomposites were more significant than that of RGO, indicating that the disorder amount was more remarkable. A more defective one can help to adsorb more hydrogen.

With a ramping heating rate of 10 °C min^{-1}, TGA was conducted between 50 and 700 °C. Figure 3 shows the TGA curves for the RGO and RGO/h-BN nanocomposites. For the RGO (see Fig. 3a), the initial weight loss (200 and 230 °C)

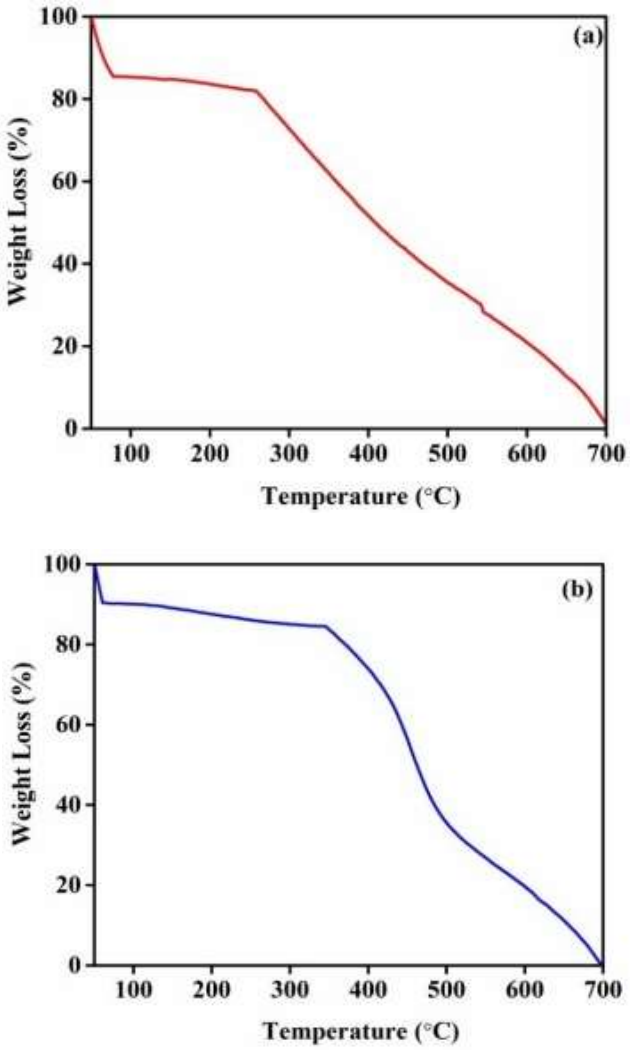

Fig. 3. TGA curves of (a) RGO and (b) RGO/h-BN nanocomposite.

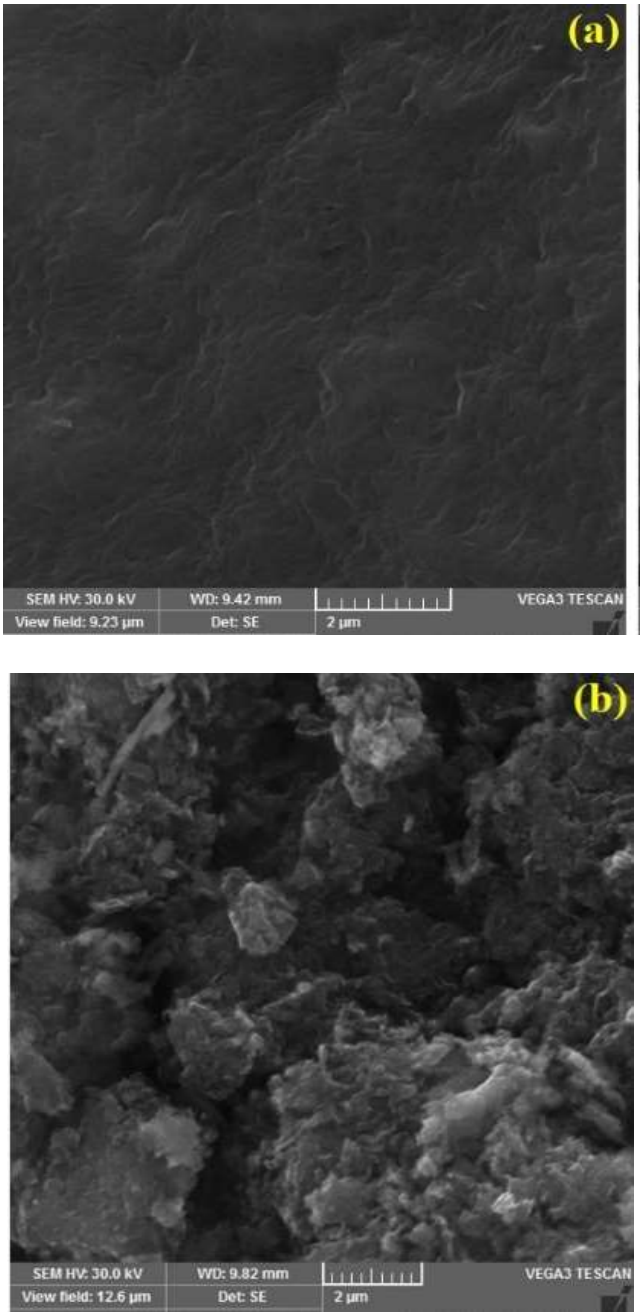

Fig. 4. SEM images of the (a) RGO (b) RGO/h-BN nanocomposite.

was due to the disintegration of less stable oxygen-containing functional groups, whereas the second gradual weight loss (230 °C to 700 °C) was prompted by the removal of more stable functional groups from the RGO sheets. It began above 330 °C in the case of the RGO/h-BN (see Fig. 3b). Compared to RGO nanostructures, the RGO/h-BN nanocomposite could offer greater thermal stabilities. According to the findings of the TGA investigations, chemically bonding h-BN nanoparticles with RGO could significantly boost their heat stability. This outcome is in good agreement with micro-Raman and XRD assessments.

Figure 4 shows the SEM picture of the synthesized RGO and RGO/h-BN nanocomposite. The SEM photographs of RGO (Fig. 4a) revealed the crumpled and wrinkled graphene sheet structure morphology. From Fig. 4b (RGO/h-BN nanocomposite), the uniformly decorated spherical shape and noticeable agglomeration of h-BN nanoparticles on the surface of RGO sheets were obtained. This result confirmed

that the RGO sheets were anchored with the h-BN nanoparticles, in agreement with XRD and micro-Raman studies.

Hydrogen Adsorption Analysis

The amount of hydrogen stored in the prepared nanocomposite was determined by the CHNS-elemental analysis. Figure 5 shows how much hydrogen could be absorbed in the RGO and RGO/h-BN nanocomposite for 10 min at 1 l min^{-1} flow rate and a constant hydrogenation temperature of 100 °C. The hydrogen adsorption capacities of RGO and RGO/h-BN nanocomposites were 0.8 and 2.1 wt%, respectively. This finding indicates that adding the h-BN nanoparticles improves the RGO's storage capability. The explanation for the improved hydrogen-storage capacity of the RGO/h-BN is that (i) more hydrogen was adsorbed on the two-dimensional surface of the RGO, (ii) more h-BN nanoparticles might be present due to the interlayer, and (iii) more h-BN nanoparticles might be present due to the dipolar nature of B-N. According to the CHNS elemental analysis, the RGO/h-BN nanocomposite was a more effective hydrogen storage system than pristine RGO.

Hydrogen Desorption Analysis

The TGA results revealed the desorption profile of hydrogen. The hydrogenated RGO and RGO/h-BN nanocomposite TG plots are shown in Figs. 6a and b, respectively, and the region linked to the hydrogen desorption is shown in the inset. According to Fig. 6b, the hydrogenated RGO/h-BN nanocomposite's TG curve has two degradation stages: one from 115 to 149 °C and another from above 330 °C. The nanocomposite's first weight loss of 2.1 wt% is ascribed to the desorption of hydrogen that had been stored there. RGO started to disintegrate, and the second weight reduction began at over 330 °C. Thus, it is confirmed that the first weight reduction in the nanocomposite was due to the release of hydrogen that had been stored rather than by the hydrogen in the RGO/h-BN. The RGO (see Fig. 6a) showed a weight reduction of 0.8 wt.% in the 109-140 ºC.

Using the Van't Hoff equation, hydrogen's binding energy (E_B) was determined from the desorption temperature [17].

$$T_m = \frac{E_B}{K_B}\left(\frac{\Delta S}{R} - \ln P\right)^{-1} \quad (2)$$

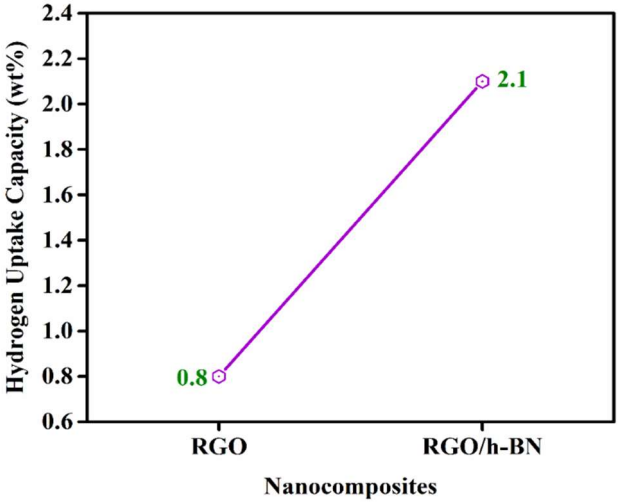

Fig. 5. Hydrogen adsorption of RGO and RGO/h-BN nanocomposite at 100 ºC at 1 l min^{-1} flow rate.

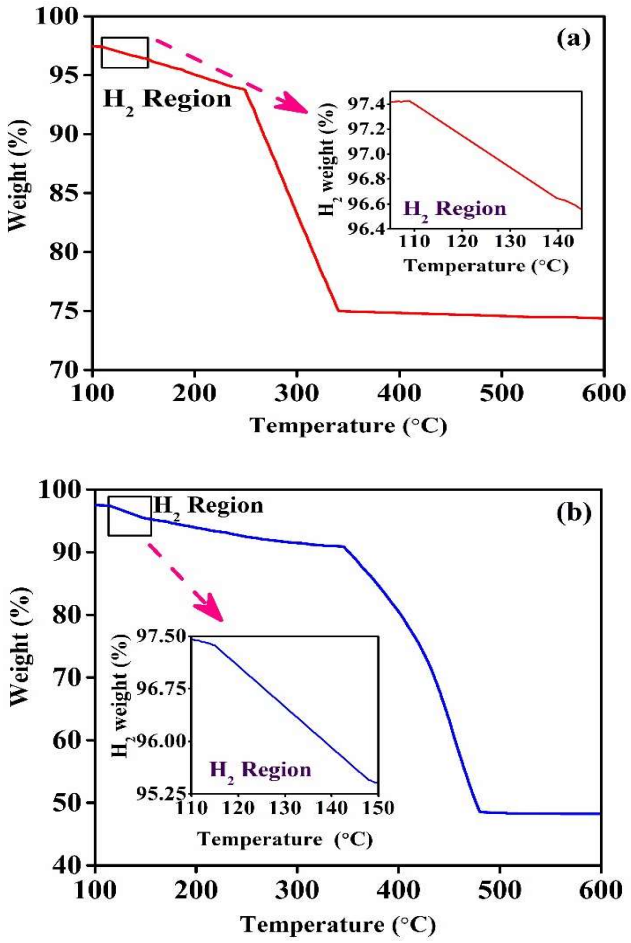

Fig. 6. TGA curves of (a) RGO (b) RGO/h-BN hybrid nanocomposite.

K_B, ΔS, R, and P are Boltzmann constant, change in H_2 entropy from gas to liquid phase, gas constant, and equilibrium pressure of 1 atm, respectively. The binding energy of RGO/h-BN nanocomposites are 0.30 eV and 0.33 eV for the desorption temperatures of 115 ºC and 149 ºC, respectively.

Besides, the desorption activation energy (E_d) was computed using Eq. (3) [17]

$$\ln\left(\frac{T_m^2}{\beta}\right) = \frac{E_d}{RT_m} \quad (3)$$

The activation energy of RGO/h-BN nanocomposite was estimated as 20.12 kJ mol^{-1} and 22.24 kJ mol^{-1} for 115 ºC and 149 ºC desorption temperatures, respectively. Table 1 shows the hydrogen-desorption activation energy, hydrogen-desorption temperature, and the binding energies of the RGO and RGO/h-BN nanocomposites. As a result, at room temperature, the hydrogenated RGO and RGO/h-BN retained their stored hydrogen stability. According to Table 1, the RGO and RGO/h-BN had weak chemisorption for hydrogen storage. The binding energy (E_B) of stored hydrogen in a perfect hydrogen-storage system of fuel cell application should be between 0.2 and 0.4 eV [17]. The prepared RGO and RGO/h-BN nanocomposite's hydrogen binding energy was within this recommended US-DOE range. The RGO/h-BN can therefore be utilized in fuel cell applications.

The amount of hydrogen desorbed by the prepared RGO and RGO/h-BN nanocomposites was equivalent to the amount of hydrogen stored, as shown by CHNS elemental analysis and TGA. As a result, the created RGO/h-BN nanocomposite showed 100% desorption.

Cyclic Performance of Hydrogen Storage Capacity

The produced RGO/h-BN nanocomposite underwent four hydrogenation cycles to test its cyclic stability. After the first hydrogenation cycle, RGO/h-BN was heated for 30 min at 200 °C to release the contained hydrogen. After that, the sample was once more hydrogenated using a Sievert-style hydrogenation setup at 100 °C, and the CHNS elemental analysis was used to determine the sample's hydrogen absorption capacity. This process was repeated four times, and the final outcome is depicted in Fig. 7. According to this finding, the RGO/h-BN nanocomposite showed 76.2 wt% hydrogen absorption capability during the hydrogenations' fourth cycle.

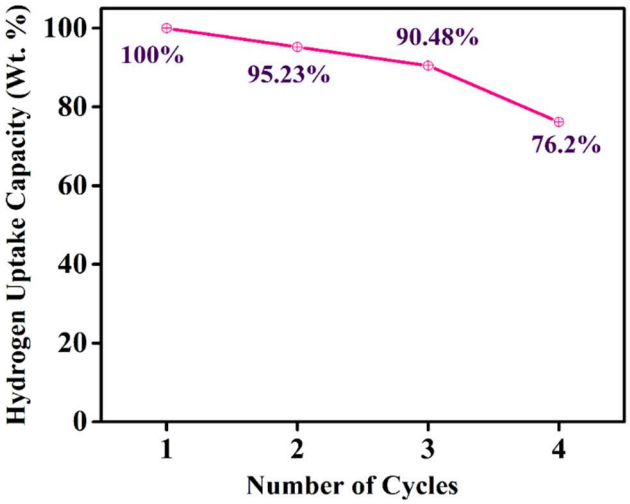

Fig. 7. Cyclic hydrogen uptake capacity of rGO/h-BN nanocomposite.

Structural Stability of RGO/h-BN Nanocomposite

After cyclic hydrogen storage capacity performance, the stability of the RGO/h-BN structure was examined through micro-Raman analysis. After the fourth cycle of hydrogenations, the RGO/h-BN nanocomposite was heated to 200 °C. Then the sample was subjected to micro-Raman analysis, depicted in Fig. 8. From Fig. 8, the I_D/I_G ratio after the fourth cycle of hydrogenations was 1.64. This signifies that the I_D/I_G ratio is slightly increased and comparable with

Table 1. Desorption Characteristics Parameters of RGO and RGO/h-BN

Nanocomposite	H_2 (wt.%)	T_m (ºC)	E_d (kJ mol^{-1})	E_B (eV)
RGO	0.8	109-140	17.86-27.12	0.29-0.32
RGO/h-BN	2.1	115-149	20.12-22.24	0.30-0.33

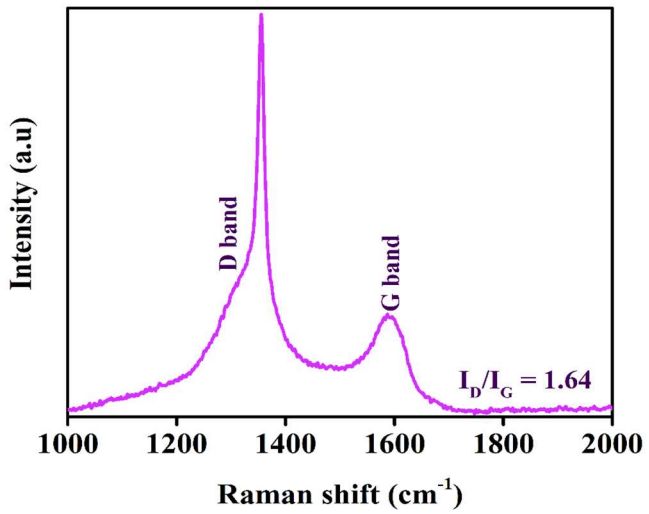

Fig. 8. Raman spectra of dehydrogenated rGO/h-BN nanocomposite after the fourth cycles.

freshly prepared RGO/h-BN nanocomposite. The outcome confirms the RGO/h-BN retains the structure stability and releases stored hydrogen alone.

CONCLUSION

RGO (Reduced graphene oxide) and h-BN (hexagonal boron nitride) nanoparticles-decorated RGO nanocomposites (RGO/h-BN) were synthesized, and their hydrogen-storage performance was examined. The sonication assistance liquid-phase exfoliation approach was used to make RGO/h-BN nanocomposites, while the modified Hummer's process was applied to prepare graphene oxide (GO). The structural and morphological characterization of prepared RGO and RGO/h-BN nanocomposite was performed through XRD, micro-Raman, TGA, and SEM analysis. The micro-Raman and XRD studies proved the purity and incorporation of the h-BN nanoparticles into the RGO sheets. Results of Raman spectra showed more structural disorder for the prepared RGO sheets and RGO/h-BN nanocomposite. The SEM analysis indicated that the h-BN nanoparticles anchored on the surface of the RGO sheet. In the Sieverts-like hydrogen method, the RGO and RGO/h-BN nanocomposites' hydrogen storage capacity was carried out at 100 ºC, and 0.8 and 2.1 wt.% was achieved, respectively. The hydrogenated RGO and RGO/h-BN nanocomposites were stable and did not release stored hydrogen at room temperature. For the RGO/h-BN nanocomposites, the stored hydrogen (capacity of 2.1 wt.%) were released in a temperature range of 115-149 ºC and exhibited 100% desorption. It was discovered that the hydrogen binding (0.32 eV) in RGO/h-BN nanocomposite had a weak chemisorption nature. Hence, the present prepared RGO/h-BN nanocomposite offers a facile, low-cost synthesis route, and excellent hydrogen storage capacity. The binding energy falls in the proposed US-DOE target, exhibiting the potential solid-state hydrogen-storage system for fuel cell applications.

REFERENCES

[1] Pandith, A.; Jayaprakash, G. K.; ALOthman, Z. A., Surface-modified CuO nanoparticles for photocatalysis and highly efficient energy storage devices. *Environ. Sci. Pollut. Res.* **2023**, *30*, 43320-43330, DOI: 10.1007/s11356-023-25131-4.

[2] Rajendrachari, S.; Jayaprakash, G. K.; Pandith, A.; Karaoglanli, A. C.; Uzun, O., Electrocatalytic Investigation by Improving the Charge Kinetics between Carbon Electrodes and Dopamine Using Bio-Synthesized CuO Nanoparticles. *Catalysts* **2022**, *12*, 994, DOI: 10.3390/catal12090994.

[3] Nagarajarao, S. H.; Nandagudi, A.; Viswanatha, R.; Basavaraja, B. M.; Santosh, M.S.; Praveen, B. M.; Pandith, A., Recent Developments in Supercapacitor Electrodes: A Mini Review. *Chem. Engineering* **2022**, *6*, 5, DOI: 10.3390/chemengineering6010005.

[4] Eberle, U.; Felderhoff, M.; Schuth, F., Chemical and Physical Solutions for Hydrogen Storage. *Angew. Chem., Int. Ed.* **2009**, *48*, 6608-6630, DOI: 10.1002/anie.200806293.

[5] Owens, D.; Han, A.; Sun, L.; Mao, Y., Synthesis of VTMS(X)-HMS-3 mesoporous ordered silica for hydrogen storage. *Int. J. Hydrogen Energy* **2015**, *40*, 2736-2741, DOI: 10.1016/j.ijhydene.2014.12.100.

[6] Alesaadi, S. J.; Sabzi, F., Hydrogen storage in a series of Zn based MOFs studied by Sanchez-Lacombe equation of state. *Int. J. Hydrogen Energy* **2015**, *40*, 1651-1656, DOI: 10.1016/j.ijhydene.2014.12.008.

[7] Churchard, A. J.; Banach, E.; Borgschulte, A.; Caputo,

R.; Chen, J. -C.; Clary, D.; Fijalkowski, K. J.; Geerlings, H.; Genova, R. V.; Grochala, W.; Jaron, T.; Juanes-Marcos, J. C.; Kasemo, B.; Kroes, G. -J.; Ljubic, I.; Naujoks, N.; Norskov, J. K.; Olsen, R. A.; Pendolino, F.; Remhof, A.; Romanszki, L.; Tekin, A.; Vegge, T.; Zachi M.; Zuttelc, A., A multifaceted approach to hydrogen storage. *Phys. Chem. Chem. Phys.* **2011**, *13*, 16955-16972, DOI: 10.1039/C1CP22312G.

[8] Jia, Y.; Sun, C.; Shen, S.; Zou, J.; Mao S. S.; Yao, X., Combination of nanosizing and interfacial effect: future perspective for designing Mg-based nanomaterials for hydrogen storage. *Renewable Sustainable Energy Rev.* **2015**, *44*, 289-303, DOI: 10.1016/j.rser.2014.12.032.

[9] Nagar, R.; Srivastava, S.; Hudson, S. L.; Amaya, S. L.; Tanna, A.; Sharma, M.; Achayalingam, R.; Sonkaria, S.; Kare, V.; Srinivasan, S. S., Recent developments in state-of-the-art hydrogen energy technologies-Review of hydrogen storage materials. *Solar Compass* **2023**, *5*, 100033, DOI: 10.1016/j.solcom.2023.100033.

[10] Alsharabi, R. M.; Rai, S.; Mohammed, H. Y.; Farea, M. A.; Srinivasan, S.; Saxena, P. S.; Srivastava, A., A comprehensive review on graphene-based materials as biosensors for cancer detection, *Oxf. Open Mater. Sci.* **2023**, *3*, itac013, DOI: 10.1093/oxfmat/itac013.

[11] Wang, L.; Stuckert, N. R.; Yang, R. T.; Unique Hydrogen Adsorption Properties of Graphene. *AIChE J.* **2011**, *57*, 2902-2908, DOI: 10.1002/aic.12470.

[12] Srinivas, G.; Zhu, Y.; Piner, R.; Skipper, N.; Ellerby M.; Ruoff, R., Synthesis of graphene-like nanosheets and their hydrogen adsorption capacity. *Carbon* **2010**, *48*, 630-635, DOI: 10.1016/j.carbon.2009.10.003.

[13] Hudson, M. S. L.; Raghubanshi, H.; Awasthi, S.; Sadhasivam, T.; Bhatnager, A.; Simizu, S.; Sankar, S. G.; Srivastava, O. N., Hydrogen uptake of reduced graphene oxide and graphene sheets decorated with Fe nanoclusters. *Int. J. Hydrogen Energy* **2014**, *39*, 8311-8320, DOI: 10.1016/j.ijhydene.2014.03.118.

[14] Parambhath, V. B.; Nagar, R.; Ramaprabhu, S., Effect of Nitrogen Doping on Hydrogen Storage Capacity of Palladium Decorated Graphene. *Langmuir* **2012**, *28*, 7826-7833, DOI: 10.1021/la301232r.

[15] Muthu, R. N.; Rajashabala, S.; Kannan, R., Facile synthesis and characterization of a reduced graphene oxide/halloysite nanotubes/hexagonal boron nitride (RGO/HNT/h-BN) hybrid nanocomposite and its potential application in hydrogen storage. *RSC Adv.* **2016**, *6*, 79072, DOI: 10.1039/C6RA13865A.

[16] Weng, Q.; Wang, X.; Zhi, C.; Bando Y.; Golberg, D., Boron Nitride Porous Microbelts for Hydrogen Storage. *ACS Nano* **2013**, *7*, 1558-1565, DOI: 10.1021/nn305320v.

[17] Muthu, R. N.; Rajashabala, S.; Kannan, R., Hexagonal boron nitride (h-BN) nanoparticles decorated multi-walled carbon nanotubes (MWCNT) for hydrogen storage. *Renewable Energy* **2016**, *85*, 387-394, DOI: 10.1016/j.renene.2015.06.056.

[18] Muthu, R. N.; Rajashabala, S.; Kannan, R., Synthesis, characterization of hexagonal boron nitride nanoparticles decorated halloysite nanoclay composite and its application as hydrogen storage medium. *Renewable Energy* **2016**, *90*, 554-564, DOI: 10.1016/j.renene.2016.01.026.

[19] Reddy, A. L. M.; Tanur A. E.; Walker, G. C., Synthesis and hydrogen storage properties of different types of boron nitride nanostructures. *Int. J. Hydrogen Energy* **2010**, *35*, 4138-4143, DOI: 10.1016/j.ijhydene.2010.01.072.

[20] Tang, C.; Bando, Y.; Ding, X.; Qi S.; Golberg, D., Catalyzed Collapse and Enhanced Hydrogen Storage of BN Nanotubes. *J. Am. Chem. Soc.* **2002**, *124*, 14550-14551, DOI: 10.1021/ja028051e.

[21] Li, J.; Lin, J.; Xu, X.; Zhang, X.; Xue, Y.; Mi, J.; Mo, Z.; Fan, Y.; Hu, L.; Yang, X.; Zhang, J.; Meng, F.; Yuan, S.; Tang, C., Porous boron nitride with a high surface area: hydrogen storage and water treatment. *Nanotechnology* **2013**, *24*, 155603. DOI: 10.1088/0957-4484/24/15/155603.

[22] Li, F.; Gao, J.; Zhang, J.; Xu, F.; Zhao, J.; Sun, L., Graphene oxide and lithium amidoborane: a new way to bridge chemical and physical approaches for hydrogen storage. *J. Mater. Chem. A* **2013**, *1*, 8016-8022, DOI: 10.1039/C3TA10800G.

[23] Muthu, R. N.; Tatiparti, S. S. V., Electrode and symmetric supercapacitor device performance of boron-incorporated reduced graphene oxide synthesized by electrochemical exfoliation. *Energy Storage.* **2020**, e134, DOI: 10.1002/est2.134.

[24] Das, A. K.; Srivastav, M.; Layek, R. K.; Uddin, M. E.;

Jung, D.; Kima, N. H.; Lee, J. H., Iodide-mediated room temperature reduction of graphene oxide: a rapid chemical route for the synthesis of a bifunctional electrocatalyst. *J. Mater. Chem. A* **2014**, *2*, 1332-1340, DOI: 10.1039/C3TA13688D.

[25] Dey, R. S.; Hajra, S.; Sahu, R. K.; Raj, R.; Panigrahi, M. K., A rapid room temperature chemical route for the synthesis of graphene: metal-mediated reduction of graphene oxide. *Chem. Commun.* **2012**, *48*, 1787-1789, DOI: 10.1039/C2CC16031E.

[26] Gehk, R.; Perry, C. H., Normal Modes in Hexagonal Boron Nitride. *Phys. Rev.* **1966**, *146*, 543-547, DOI: 10.1103/PhysRev.146.543.